

Millicharged particles at electron colliders

Jinhan Liang,¹ Zuowei Liu,^{1,2,3,*} Yue Ma,⁴ and Yu Zhang^{5,6}

¹Department of Physics, Nanjing University, Nanjing 210093, China

²Center for High Energy Physics, Peking University, Beijing 100871, China

³CAS Center for Excellence in Particle Physics, Beijing 100049, China

⁴Kuang Yaming Honors School, Nanjing University, Nanjing 210023, China

⁵Institutes of Physical Science and Information Technology, Anhui University, Hefei 230601, China

⁶School of Physics and Materials Science, Anhui University, Hefei 230601, China

We propose to search for millicharged particles in electron colliders operated with the center-of-mass energies at $\mathcal{O}(1-10)$ GeV, which include Belle II, BESIII, BaBar, and also the proposed experiment STCF. We use the monophoton final state to probe the parameter space of millicharged particles at electron colliders. We find that electron colliders have sensitivity to the previously unexplored parameter space for millicharged particles with MeV-GeV mass: $\epsilon \lesssim \mathcal{O}(10^{-1})$ for $0.5 \text{ GeV} \lesssim m \lesssim 3.5 \text{ GeV}$ in BaBar, $\epsilon \lesssim \mathcal{O}(10^{-3})$ for $0.1 \text{ GeV} \lesssim m \lesssim 1.5 \text{ GeV}$ in BESIII, $\epsilon \lesssim 10^{-3} - 10^{-2}$ for $0.1 \text{ GeV} \lesssim m \lesssim 4 \text{ GeV}$ in Belle II, and $\epsilon \lesssim \mathcal{O}(10^{-4})$ for $1 \text{ MeV} \lesssim m \lesssim 1 \text{ GeV}$ in STCF.

INTRODUCTION

Although anomaly cancellations link the electric charges of the standard model (SM) fermions [1], in principle, there is no such constraint for particles beyond the SM (BSM). For example, particles with arbitrarily small electric charge can naturally arise in models where hidden sectors particles interact with the SM particles via kinetic mixing [2–4], or via Stueckelberg mixing [5–7]. A variety of experiments and theoretical investigations have been carried out to search for BSM particles with electric charge significantly smaller than the electron, which we refer to as millicharged particles (MCP). The constraints on MCP come both from terrestrial particle accelerators and from astrophysical processes. Particle accelerator constraints on MCP include E613 [8, 9], SLAC electron beam dump experiment [10], neutrino experiments [8, 11–15], LHC [16–18], LDMX [19], BESIII [20], and NA64 [21, 22]; some of the earlier collider constraints have been summarized in [23]. Astrophysical constraints include white dwarf [23–25], supernova [25–27], CMB [28, 29], BBN [23, 25, 30–32], red giants [23, 24, 30, 31], and Sun [32].

Recently, the 21 cm signal measured by the EDGES experiment indicates that the universe is colder than expected during the cosmic dawn [33]. Millicharged dark matter (DM) can provide cooling to the cosmic hydrogens leading to the strong 21 cm absorption signal [34–41].

In this paper, we study the experimental sensitivity on MCP from electron colliders. The constraint on MCP from the BESIII experiment has been recently studied in [20]; here we extend the analysis to other electron colliders operated the GeV scale, including Belle II, BaBar, and also the proposed experiment, the Super Tau Charm Factory (STCF). Unlike the DM constraints which assume a sufficient amount of millicharged DM in our universe, particle colliders can provide robust constraints on the MCP which is independent on its composition in the universe. At the MeV-GeV scale, the leading con-

straints on MCP come from colliders [23], SLAC [10], and LSND/MiniBooNE [12]. We find that electron colliders can probe the previously unexplored MCP parameter space with MeV-GeV mass. Our analysis also has a direct impact on millicharged DM models that are invoked to explain the 21 cm anomaly.

ELECTRON COLLIDER SIGNALS

In our analysis, we assume that the MCP is a Dirac fermion which is charged under the SM photon via the interaction Lagrangian, $\mathcal{L}_{\text{int}} = e\epsilon A_\mu \bar{\chi}\gamma^\mu\chi$, where χ is the MCP, A_μ is the SM photon. The analysis presented here can be easily extended to MCPs with other spins.

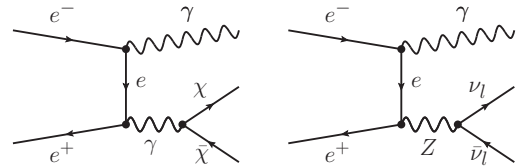


Figure 1: Feynman diagrams for the process $e^+e^- \rightarrow \chi\bar{\chi}\gamma$ (left) and $e^+e^- \rightarrow \nu\bar{\nu}\gamma$ (right).

Because the ionization signal of the MCP is typically undetectable in collider experiments, one thus relies on the visible final state particles produced in association with MCPs for the detection. Thus we use the monophoton final state in electron colliders to search for MCPs [20]. The Feynman diagram for the signal process is shown in Fig. (1). The maximum photon energy is $E_\gamma^{\text{max}} = (s - 4m_\chi^2)/(2\sqrt{s})$.

Belle II is operated on SuperKEKB which collides 7 GeV electrons with 4 GeV positrons [42]. SuperKEKB has a design luminosity of $8 \times 10^{35} \text{ cm}^{-2} \text{ s}^{-1}$ and expects to collect 50 ab^{-1} integrated luminosity with 8-year data takings [42]. An upgrade with five times more luminosity

is also anticipated with Belle II [43]. The BESIII detector is located at the BEPCII with the beam energy ranging from 1.0 GeV to 2.3 GeV and luminosity of $10^{33} \text{ cm}^{-2} \text{ s}^{-1}$ [44]. STCF is a proposed experiment which collides electron with positron at the center-of-mass energies in the range 2-7 GeV, with the peak luminosity $\mathcal{O}(10^{35}) \text{ cm}^{-2} \text{ s}^{-1}$ at 4 GeV [45]. An integrated luminosity up to 20 ab^{-1} is expected to be accumulated with a 10-year STCF runnings, assuming 9-month running time each year and 90% data taking efficiency [45]. The BaBar detector is operated at the PEP-II e^+e^- collider from 1999 to 2008 with most data collected near $\sqrt{s} = 10.58 \text{ GeV}$ (the $\Upsilon(4S)$ resonance) [46].

There are two types of monophoton backgrounds: irreducible background and reducible background. The irreducible monophoton background is the SM final state containing one photon and two neutrinos; one of the irreducible background processes is shown in Fig. (1). The reducible monophoton background arises when a photon is produced in the final state together with several other visible particles which are however not detected due to the limitations of the detector acceptance. Belle II and BaBar have asymmetric detectors; BESIII and STCF have symmetric detectors. We discuss the reducible BG in detail later for each experiment, since it strongly depends on the angular coverage of the detectors.

BELLE II

In Belle II, photons and electrons can be detected in the Electromagnetic Calorimeter (ECL), which consists of three segments: forward endcap with $12.4^\circ < \theta < 31.4^\circ$, barrel with $32.2^\circ < \theta < 128.7^\circ$, and backward endcap $130.7^\circ < \theta < 155.1^\circ$ in the lab frame [42]. There are two important monophoton reducible backgrounds [42]: one is mainly due to the lack of polar angle coverage of the ECL near the beam directions, which is referred to as the “bBG”; the other one is mainly due to the gaps between the three segments in the ECL detector, which is referred to as the “gBG”.

In the bBG, all the final state particles except the detected monophoton are emitted with $\theta > 155.1^\circ$ or $\theta < 12.4^\circ$ in the lab frame. Some major bBG processes include $e^+e^- \rightarrow \gamma\gamma\gamma$ and $e^+e^- \rightarrow \ell^+\ell^-\gamma$ where $\ell = e, \mu, \tau$; the final state particles with a slash on the name are emitted along the beam directions.

For symmetric detectors, such as BESIII and STCF, the maximum energy of the monophoton events in the bBG in the CM frame, E_γ^m , is given by

$$E_\gamma^m(\theta_\gamma) = \sqrt{s} \left(1 + \frac{\sin \theta_\gamma}{\sin \theta_b} \right)^{-1}, \quad (1)$$

where θ_b is the polar angle corresponding to the edge of the detector [47]. For the Belle II detector, which

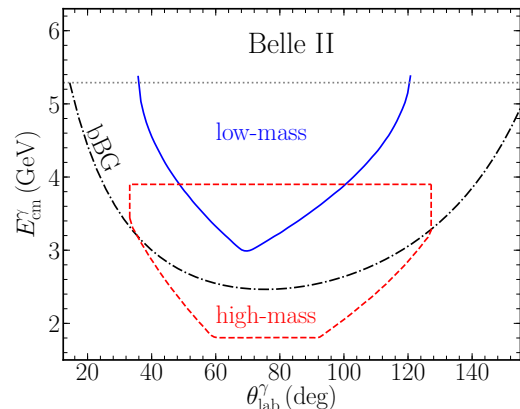


Figure 2: Monophoton phase space $E_{\text{cm}}^\gamma - \theta_{\text{lab}}^\gamma$ in Belle-II. E_{cm}^γ is the photon energy in the CM frame; $\theta_{\text{lab}}^\gamma$ is the photon polar angle with respect to the initial electron in the lab frame. We refer to the region above the blue solid line as “low-mass” region and the region enclosed by the red dashed line as the “high-mass” region. Both the “low-mass” and “high-mass” regions are taken from simulations given in Ref. [42]. The gray dotted line indicates the $\sqrt{s}/2$ value in Belle-II. The black dot-dashed line is the bBG cut.

is asymmetric, E_γ^m in the CM frame is given by (if not exceeding $\sqrt{s}/2$)

$$E_\gamma^m(\theta_\gamma) = \frac{\sqrt{s}(A \cos \theta_1 - \sin \theta_1)}{A(\cos \theta_1 - \cos \theta_\gamma) - (\sin \theta_\gamma + \sin \theta_1)} \quad (2)$$

with the maximum of where all angles are given in the CM frame, and $A = (\sin \theta_1 - \sin \theta_2)/(\cos \theta_1 - \cos \theta_2)$, with θ_1 and θ_2 being the polar angles corresponding to the edges of the ECL detector [55]. To remove the above bBG, the detector cut $E_\gamma > E_\gamma^m$ is used (hereafter the “bBG” cut), which is shown in Fig. (2).

Because the ECL gaps are significantly away from the beam direction, the monophoton energy of the gBG can be quite large in the central θ_γ region. The gBG simulations have been carried out by Ref. [42] in searching for an invisibly decaying vector boson. The dominated gBG is $e^+e^- \rightarrow \gamma\gamma\gamma(\gamma)$ with at least one final state photon emitting through the gaps [42]. For example, one major background arises when one final state photon in the process $e^+e^- \rightarrow \gamma\gamma\gamma$ escapes via the gap between the ECL barrel and the backward endcap, and the second photon is emitted along the beam direction [48]. Two different sets of detector cuts are designed by Ref. [42] to optimize the detection efficiency for different masses of the vector boson, which are shown in Fig. (2). The “low-mass” region in the monophoton phase space has few gBG events, which is applied for the vector boson with mass less than 6 GeV. However, if the vector boson mass is in the range 6 – 8 GeV, only low energy photons can be produced in

the new physics processes so that the “high-mass” cut region is preferred.

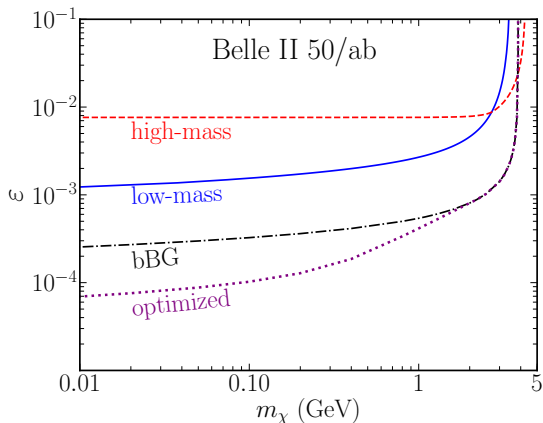


Figure 3: The expected 95% confidence level (C.L.) upper bound on millicharge at Belle II under the low-mass cut (solid) and the high-mass cut (dashed), with 50 ab^{-1} integrated luminosity. The black (purple) line corresponds to the limit using the bBG (optimized) cut.

To probe the millicharge, we define $\chi^2(\epsilon) \equiv S^2/(S+B)$ [49], where S (B) is the number of events in the signal (background) processes. The 95% confidence level (C.L.) upper bound on the millicharge, ϵ_{95} , is obtained by solving $\chi^2(\epsilon_{95}) - \chi^2(0) = 2.71$. Fig. (3) shows the expected 95% C.L. upper bound on millicharge using the “low-mass” and “high-mass” cuts with 50 ab^{-1} data. We calculate the signal and irreducible background events by integrating the differential monophoton cross sections in different regions of the phase space under different detector cuts, and assuming photon detection efficiency as 95% [42]. Our calculation shows that there are about 10900 (2280, 15230) irreducible BG events with the bBG (low-mass, high-mass) cut with 50 ab^{-1} integrated luminosity. For the reducible background, it is found that about 300 (25000) gBG events survived the low-mass (high-mass) cuts with 20 fb^{-1} integrated luminosity [42], which are rescaled according to the luminosity. The constraint with the high mass cut becomes better than the low-mass cut when the MCP mass exceeds $\sim 3 \text{ GeV}$.

We also compute the limits without gBG taking into account, in order to compare with other experiments where detailed simulations with gBG are not available. We use the bBG cut to remove the reducible background events; the BG events survived the bBG cut are due to irreducible backgrounds, if gBG is not considered. We integrated the monophoton differential cross section for MCP [20] and for SM irreducible BG [20], with the bBG cut to obtain the number of events. The 95% confidence level (C.L.) upper bound analyzed with the bBG cut is shown

in Fig. (3) where gBG is not considered; the upper bound is about five times stronger than the one when gBG is considered under the low-mass cut, for millicharged particles with mass less than 1 GeV.

BESIII AND STCF

It has been recently proposed to search for MCPs in BESIII [20]. Here we update the BESIII sensitivity by taking into account the most recent data: 1.4 (0.13, 0.5) fb^{-1} at $\sqrt{s} = 3.097$ (3.554, 3.686) GeV [50]. In BESIII, we have $\cos \theta_b = 0.95$, taking into account the coverage of MDC, EMC, and TOF [20]. We adopt the detector cuts for photons by BESIII Collaboration (hereafter the pre-selection cuts) [51]: $E_\gamma > 25 \text{ MeV}$ with $|\cos \theta| < 0.8$ or $E_\gamma > 50 \text{ MeV}$ with $0.86 < |\cos \theta| < 0.92$. We further apply the bBG cut to remove the reducible background. We compute the number of events under both pre-selection cuts and the bBG cut given in Eq. (1). We define $\chi_{\text{tot}}^2(\epsilon) = \sum_i \chi_i^2(\epsilon)$, where $\chi_i^2(\epsilon) \equiv S_i^2/(S_i + B_i)$ for each BESIII colliding energy. The 95% C.L. upper bound on millicharge from BESIII is obtained by demanding $\chi_{\text{tot}}^2(\epsilon_{95}) = \chi^2(0) + 2.71$, which is shown in Fig. (8).

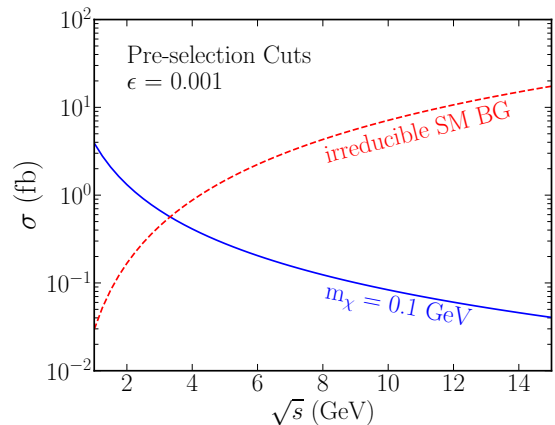


Figure 4: Monophoton cross section as a function of \sqrt{s} for MCPs (solid), and for irreducible BG (dashed). Only pre-selection cuts are applied. We use $\epsilon = 0.001$ and $m_\chi = 0.1 \text{ GeV}$ for the MCP.

A total luminosity of 20 ab^{-1} is expected at the future STCF experiment operated at $\sqrt{s} = 2-7 \text{ GeV}$. Although the STCF luminosity is a little smaller than Belle II, the smaller colliding energy in STCF enhances the sensitivity to sub-GeV MCPs. Fig. (4) shows the monophoton cross section in the new physics model and in irreducible BG; the signal to background ratio increases when the colliding energy decreases. STCF is thus the ideal experiment to search for light MCPs because of both the high inte-

grated luminosity and the relatively low colliding energy.

We use the BESIII detector parameters to analyze the constraints from STCF, because of the similarity of the two experiments. Fig. (5) shows the expected STCF limits on millicharge assuming 10 ab^{-1} luminosity at three different colliding energies. We compute the signal and irreducible background under both the pre-selection cuts and the bBG cut; the irreducible BG yields about 27 pb at $\sqrt{s} = 4 \text{ GeV}$ under these cuts. The STCF can probe $\epsilon \simeq 10^{-4}$ for mass around 10 MeV, if operated at $\sqrt{s} = 2 \text{ GeV}$ with 10 ab^{-1} data.

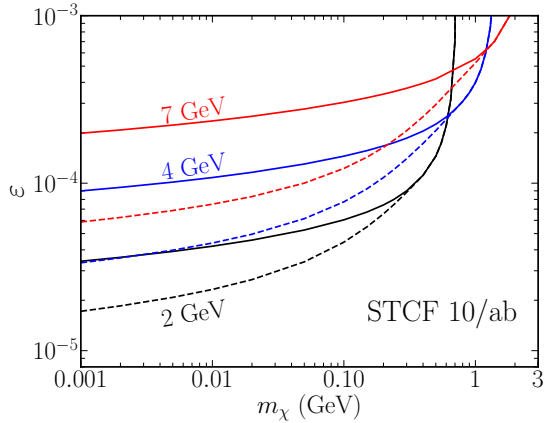


Figure 5: The expected 95% C.L. exclusion limits on millicharge at STCF at various colliding energies with 10 ab^{-1} luminosity. Solid (dashed) curves indicate the limits under the bBG (optimized) cut for $\sqrt{s} = 7, 4, 2 \text{ GeV}$ in the descending order.

BABAR

To probe MCPs, we use the monophoton events collected by BaBar collaboration [52] which were previously analyzed to search for the light scalar particle A^0 produced via $e^+e^- \rightarrow \Upsilon(3S) \rightarrow \gamma A^0$; two sets of data are analyzed in Ref. [52]: the 28 fb^{-1} ‘‘High-E’’ photons with $3.2 \text{ GeV} < E_{\text{cm}}^\gamma < 5.5 \text{ GeV}$, $-0.31 < \cos(\theta_{\text{cm}}^\gamma) < 0.6$, and $\cos(6\phi_{\text{cm}}^\gamma) < 0.96$ corresponding to the Instrumented Flux Return (IFR) fiducial; the 19 fb^{-1} ‘‘Low-E’’ photons with $2.2 \text{ GeV} < E_{\text{cm}}^\gamma < 3.7 \text{ GeV}$ and $-0.46 < \cos(\theta_{\text{cm}}^\gamma) < 0.46$.

The detector cuts used in the BaBar analysis [52] can be divided into two categories: geometric cuts and non-geometric cuts; we compute the detector efficiency separately for these two cuts, following [53]. The detector efficiency for geometric cuts in High-E (Low-E) region is about 34% (37%) for the $(1 + \cos^2 \theta_\gamma)$ angular distribution used in [52]. Because the total detector efficiency for

$e^+e^- \rightarrow \Upsilon(3S) \rightarrow \gamma A^0$ is (10-11)% (20%) in the High-E (Low-E) region [52], the detector efficiency for the non-geometric cuts (denoted as f_{NG}) is about 30% (54%) in the High-E (Low-E) region. The signal events under the High-E and Low-E detector cuts is computed via

$$N_s = \mathcal{L} f_{\text{NG}} \int d\Omega dE_\gamma^d dE_\gamma f(E_\gamma^d, E_\gamma, \delta E_\gamma) \frac{d\sigma}{dE_\gamma dz_\gamma} \quad (3)$$

where $d\sigma/(dE_\gamma dz_\gamma)$ is the differential cross section [20], $z_\gamma = \cos(\theta_\gamma)$, E_γ^d is the detected photon energy, and $\mathcal{L} = 28 \text{ (19) fb}^{-1}$ for High-E (Low-E) data [52] [46]. Here the photon energy is smeared via the crystal ball function $f(E_\gamma^d, E_\gamma, \delta E_\gamma)$ with the energy resolution $\sigma(E_\gamma)/E_\gamma = 1.5\% (E_\gamma/\text{GeV})^{1/4} \oplus 1\%$ [53].

Following Refs. [52, 53], we model the background using fitting functions: We use a crystal ball function peaked at $m_{\chi\chi} = 0$, where $m_{\chi\chi}^2 = s - 2\sqrt{s}E_\gamma$, with normalization N_1 and $N_2 \exp(c m_{\chi\chi}^2)$ for the High-E region; we use $N_3 \exp(c_1 m_{\chi\chi}^2 + c_2 m_{\chi\chi}^4)$ and a constant term N_4 for the Low-E region. The 95% C.L. upper bound on millicharge is computed using the profile likelihood method. The likelihood function we use is

$$\mathcal{L} = \max \left\{ \prod_{i=1}^{\text{bins}} \exp \left[\frac{(N_s^i + N_b^i - N_o^i)^2}{2\sigma_i^2} \right] \right\}, \quad (4)$$

where $N_s^i (N_b^i, N_o^i)$ is the number of signal (background, observed) events in bin i , and σ_i is the error bar. We use $N_1, N_2, N_3, c, c_1, c_2$ as nuisance parameters. The upper bound on millicharge from the BaBar data is shown in Fig. (6).

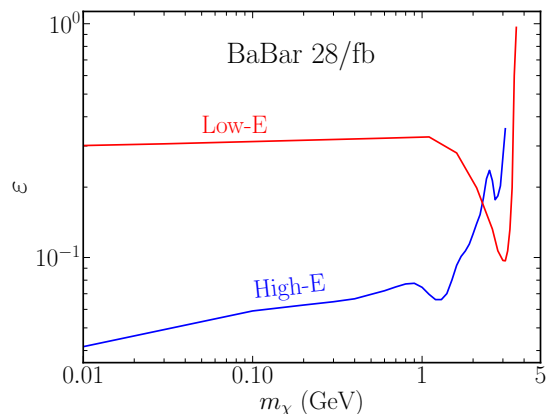


Figure 6: The 95% limits on ϵ with profile likelihood method at BaBar. The blue (red) solid line shows the limit with BaBar High-E (Low-E) data.

OPTIMIZED CUT

We further carry out a preliminary analysis in which we optimize the detector cuts by considering the irreducible background only. For the low energy electron collider, the monophoton cross section decreases with photon energy in the irreducible background, but the monophoton cross section can increase with photon energy for the MCPs. Thus, selecting photons with relatively high energy can enhance discovery sensitivity. To find the optimized cut, in addition to the bBG cut, we select photons in the range $E_\gamma^{\min} < E_\gamma < E_\gamma^{\max}$, where $E_\gamma^{\max} = (s - 4m_\chi^2)/(2\sqrt{s})$ and vary E_γ^{\min} to find the best limit on millicharge. Furthermore, the energy difference $\Delta E_\gamma \equiv E_\gamma^{\max} - E_\gamma^{\min}$ is required to be larger than the photon energy resolution σ_E , when E_γ^{\max} is more than 1 σ_E above the minimum value of the bBG cut curve.

Fig. (7) shows the ΔE_γ that gives rise to the best limit on millicharge in Belle II and STCF. For STCF, we use the photon resolution of the EMC in BESIII $\sigma_E/E = 2.3\%/\sqrt{E/\text{GeV}} \oplus 1\%$ [44], and we take $\sigma_E = 38$ MeV for light mass. For Belle II, $\sigma_E/E = 4\%(1.6\%)$ at 0.1 (8) GeV [42] and we take $\sigma_E = 128$ MeV for light mass. As shown in Fig. (7), the best ΔE_γ value is equal to the photon energy resolution for light mass. For high mass, because E_γ^{\max} starts to approach the bBG cut, ΔE_γ can become smaller than the photon energy resolution.

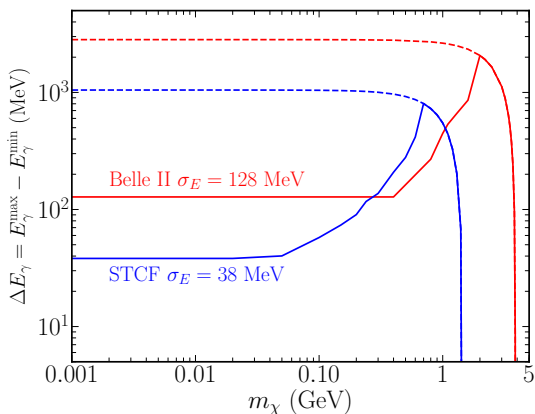


Figure 7: The ΔE_γ value that yields the best limit on millicharge in Belle II and STCF. We use 50 (20) ab^{-1} data here for Belle II (STCF). We consider $\sqrt{s} = 4$ GeV for STCF. The dashed lines indicate the bBG cuts.

RESULTS

Fig. (8) summarizes the sensitivity on millicharge ϵ from the low energy electron colliders, including Belle

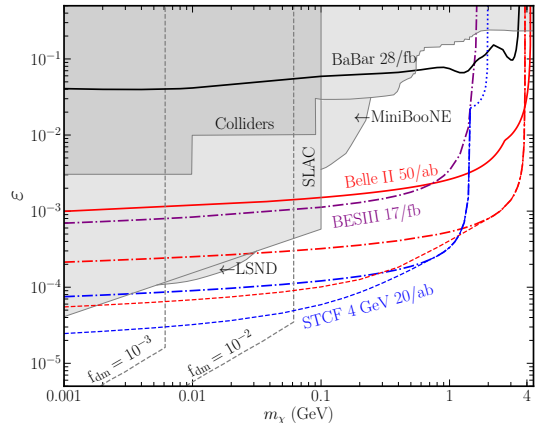


Figure 8: The expected 95% C.L. exclusion limits on MCPs at Belle II, BESIII, STCF, and BaBar. The BaBar limit (black-solid) is obtained by combining the High-E limit and Low-E limit in Fig. (6). The BESIII limit (purple-dot-dashed) is obtained by analyzing the data collected during 2011-2018. The Belle II limit (red-solid) combines the low-mass and high-mass limit in Fig. (3). The other two Belle II limits (red-dot-dashed, red-dashed) are obtained with the (bBG, optimized) cuts where only SM irreducible BG is considered. The STCF limits (blue-dot-dashed, blue-dashed) are obtained for $\sqrt{s} = 4$ GeV and 20 ab^{-1} under the (bBG, optimized) cuts where only SM irreducible BG is considered. Beyond mass ~ 1.4 GeV, we analyze monophoton signal using the pre-selection cuts to obtain the STCF limit, which is shown as the blue-dotted curve. Previous constraints including colliders [25] [17], SLAC [10], LSND [12], and MiniBooNE [12] are also presented. The parameter space of millicharged DM to explain the 21 cm anomaly [33] is also shown where $f_{\text{dm}} = 10^{-3}$ (10^{-2}) is the millicharged DM fraction [34].

II, STCF, BESIII, and BaBar. The BaBar and Belle II limits, shown as solid curves on Fig. (8), have been analyzed taking into account the various SM backgrounds. With existing data from BaBar, the previously allowed parameter space with millicharge $\epsilon \sim 10^{-1}$ and mass $\sim (1 - 3)$ GeV can be probed. Due to the higher luminosity expected at Belle II, a larger parameter space that is previously unconstrained by other experiments is going to be explored by the Belle II; with 50 ab^{-1} data, millicharge down to $\sim 10^{-2} - 10^{-3}$ for mass $\sim (0.1 - 4)$ GeV is expected to be probed by Belle II.

The STCF and BESIII limits, shown as dot-dashed curves on Fig. (8), are obtained when the background due to the gaps in the detectors are neglected. BESIII can probe new parameter space for mass > 100 MeV, with 17 fb^{-1} data collected during 2011-2018. The future STCF can probe millicharge parameter space below the SLAC experiment [10]. With 20 ab^{-1} data at $\sqrt{s} = 4$ GeV, STCF can provide leading constraints on millicharge, $\epsilon \lesssim \mathcal{O}(10^{-4})$ for mass from 3 MeV to about

1 GeV. The expected limit from STCF also eliminates some regions of the MCP parameter space where the 21 cm anomaly could be explained due to cooling from millicharged DM.

In addition to the ISR process in Fig. (1), the $\chi\chi\gamma$ final state can also occur in meson decays which can improve the sensitivity for the low mass region. However, this is beyond the scope of this work. Under the bBG cut, STCF loses sensitivity to MCP when $m_\chi \gtrsim 1.5$ GeV, since $E_\gamma^{\max} = (s - 4m_\chi^2)/(2\sqrt{s})$ is now lower than the minimum energy of the bBG cut. To estimate the STCF sensitivity for $m_\chi \gtrsim 1.5$ GeV, we only apply the pre-selection cuts; the dominant BG now is due to the $e^+e^- \rightarrow \phi^+\phi^-\gamma$ process. The STCF limit in the high mass region is shown as the blue dotted curve in Fig. (8).

To compare the capability of probing the parameter space from different experiments, we also present a Belle II limit (dot-dashed curve) with gBG omitted. Although the STCF luminosity is lower than Belle II, STCF has better sensitivity in probing the low mass region ($m \lesssim 1$ GeV) than Belle II. This is because STCF is operated at a lower colliding energy where the monophoton cross section in MCP (SM) is larger (smaller) than Belle II. The one order of magnitude difference in sensitivity between the two Belle II limits, the solid curve and the dot-dashed curve in Fig. (8), shows that the control on gGB is very important in probing the MCP parameter space. Since the dot-dashed curves in Fig. (8) are obtained without gBG, the actual limits should be weaker when gBG is taken into account. However, if the reducible background due to gaps in the detector can be significantly suppressed in the future STCF experiment, for instance with a new sub-detector that can detect the particles emitting from the gaps in ECL, the one order of magnitude increase in sensitivity from Belle II to STCF could be achieved. We further computed the limits with the optimized detector cuts, shown as dashed curves in Fig. (8). The optimized detector cuts can further enhance the sensitivity of STCF and Belle II in probing the low mass region.

SUMMARY

In this paper, we analyzed the sensitivity to millicharged particles from four different electron colliders operated at the GeV scale: BaBar, Belle II, BESIII, and STCF. By reanalyzing the 28 fb⁻¹ monophoton data collected by BaBar, one is able to eliminate some currently allowed millicharge parameter space for $\sim(0.5-3.5)$ GeV mass. The BESIII experiment can probe an even larger region of parameter space than BaBar, owing to the lower colliding energy. The expected limit on MCP from BESIII is near $\epsilon \sim 10^{-3}$ for 100 MeV mass. Projected limits with Belle II and STCF experiments are also analyzed. It is found that Belle II can probe millicharge down to

$\epsilon \sim 10^{-3} - 10^{-2}$ for 0.1 GeV $\lesssim m \lesssim 4$ GeV. The future STCF can further improve the sensitivity to low mass MCP than Belle II because it is operated at lower energy. Millicharge $\epsilon \lesssim \mathcal{O}(10^{-4})$ for mass from 3 MeV to about 1 GeV can be probed by the future STCF experiment; this excludes some of the parameter space for explaining the 21 cm anomaly. The sensitivities computed for BESIII and STCF are obtained without taking into account the gap backgrounds. The more accurate limits require full detailed detector simulations, which is beyond the scope of this work.

ACKNOWLEDGEMENT

We thank Shenjian Chen, Van Que Tran, Jingjing Xu, and Lei Zhang for discussions and correspondence. The work is supported in part by the National Natural Science Foundation of China under Grant Nos. 11775109, U1738134, and 11805001, and by the National Recruitment Program for Young Professionals.

Crystal ball function

The normalized crystal ball function is given by [54]

$$f(x, \bar{x}, \sigma) = N \begin{cases} \exp\left(-\frac{(x-\bar{x})^2}{2\sigma^2}\right), & \text{for } \frac{x-\bar{x}}{\sigma} > -\alpha \\ A\left(B - \frac{x-\bar{x}}{\sigma}\right)^{-n}, & \text{for } \frac{x-\bar{x}}{\sigma} \leq -\alpha \end{cases} \quad (5)$$

where

$$\begin{aligned} A &= \left(\frac{n}{|\alpha|}\right)^n \exp\left(-\frac{|\alpha|^2}{2}\right), \\ B &= \frac{n}{|\alpha|} - |\alpha|, \\ N &= \frac{1}{\sigma(C+D)}, \\ C &= \frac{n}{|\alpha|} \frac{1}{n-1} \exp\left(-\frac{|\alpha|^2}{2}\right), \\ D &= \sqrt{\frac{\pi}{2}} \left(1 + \operatorname{erf}\left(\frac{|\alpha|}{\sqrt{2}}\right)\right). \end{aligned}$$

We use $\alpha = 0.811$ and $n = 1.79$ for BaBar [53].

Maximum monophoton energy in reducible BG

The maximum energy of the monophoton occurs when both final state e^\pm are emitted at the boundary of ECL and are opposite to the photon in the transverse plane. Thus the energy-momentum conservation in the CM frame gives rise to

$$E_\gamma^m \sin \theta_\gamma - E_1 \sin \theta_1 - E_2 \sin \theta_2 = 0 \quad (6)$$

$$E_\gamma^m \cos \theta_\gamma + E_1 \cos \theta_1 + E_2 \cos \theta_2 = 0 \quad (7)$$

$$E_\gamma^m + E_1 + E_2 = \sqrt{s}, \quad (8)$$

where E_1 and E_2 are the e^\pm energies, and θ_1 and θ_2 are the polar angles corresponding to the boundary of the ECL. The solution for E_γ^m from the above equations yields Eq. (2). Note that the monophoton energy cannot exceed $\sqrt{s}/2$.

* Electronic address: zuoweiliu@nju.edu.cn

- [1] C. Q. Geng and R. E. Marshak, Phys. Rev. D **39**, 693 (1989).
- [2] B. Holdom, Phys. Lett. **166B** (1986) 196.
- [3] B. Holdom, Phys. Lett. B **178** (1986) 65.
- [4] R. Foot and X. G. He, Phys. Lett. B **267**, 509 (1991).
- [5] B. Kors and P. Nath, Phys. Lett. B **586**, 366 (2004) [hep-ph/0402047].
- [6] K. Cheung and T. C. Yuan, JHEP **0703**, 120 (2007) [hep-ph/0701107].
- [7] D. Feldman, Z. Liu and P. Nath, Phys. Rev. D **75** (2007) 115001 [hep-ph/0702123 [HEP-PH]].
- [8] E. Golowich and R. W. Robinett, Phys. Rev. D **35**, 391 (1987).
- [9] D. E. Soper, M. Spannowsky, C. J. Wallace and T. M. P. Tait, Phys. Rev. D **90**, no. 11, 115005 (2014) [arXiv:1407.2623 [hep-ph]].
- [10] A. A. Prinz *et al.*, Phys. Rev. Lett. **81**, 1175 (1998) [hep-ex/9804008].
- [11] S. N. Gninenko, N. V. Krasnikov and A. Rubbia, Phys. Rev. D **75**, 075014 (2007) [hep-ph/0612203].
- [12] G. Magill, R. Plestid, M. Pospelov and Y. D. Tsai, Phys. Rev. Lett. **122**, no. 7, 071801 (2019) [arXiv:1806.03310 [hep-ph]].
- [13] K. J. Kelly and Y. D. Tsai, arXiv:1812.03998 [hep-ph].
- [14] L. Singh *et al.* [TEXONO Collaboration], Phys. Rev. D **99**, no. 3, 032009 (2019) [arXiv:1808.02719 [hep-ph]].
- [15] R. Harnik, Z. Liu and O. Palamara, JHEP **1907**, 170 (2019) [arXiv:1902.03246 [hep-ph]].
- [16] J. Jaeckel, M. Jankowiak and M. Spannowsky, Phys. Dark Univ. **2**, 111 (2013) [arXiv:1212.3620 [hep-ph]].
- [17] A. Haas, C. S. Hill, E. Izaguirre and I. Yavin, Phys. Lett. B **746**, 117 (2015) [arXiv:1410.6816 [hep-ph]].
- [18] E. Izaguirre and I. Yavin, Phys. Rev. D **92**, no. 3, 035014 (2015) [arXiv:1506.04760 [hep-ph]].
- [19] A. Berlin, N. Blinov, G. Krnjaic, P. Schuster and N. Toro, Phys. Rev. D **99**, no. 7, 075001 (2019) [arXiv:1807.01730 [hep-ph]].
- [20] Z. Liu and Y. Zhang, Phys. Rev. D **99**, no. 1, 015004 (2019) [arXiv:1808.00983 [hep-ph]].
- [21] S. N. Gninenko, D. V. Kirpichnikov and N. V. Krasnikov, arXiv:1810.06856 [hep-ph].
- [22] X. Chu, J. Pradler and L. Semmelrock, Phys. Rev. D **99**, no. 1, 015040 (2019) [arXiv:1811.04095 [hep-ph]].
- [23] S. Davidson, B. Campbell and D. C. Bailey, Phys. Rev. D **43**, 2314 (1991).
- [24] M. I. Dobroliubov and A. Y. Ignatiev, Phys. Rev. Lett. **65**, 679 (1990).
- [25] S. Davidson, S. Hannestad and G. Raffelt, JHEP **0005**, 003 (2000) [hep-ph/0001179].
- [26] R. N. Mohapatra and I. Z. Rothstein, Phys. Lett. B **247**, 593 (1990).
- [27] J. H. Chang, R. Essig and S. D. McDermott, JHEP **1809**, 051 (2018) [arXiv:1803.00993 [hep-ph]].
- [28] S. L. Dubovsky, D. S. Gorbunov and G. I. Rubtsov, JETP Lett. **79**, 1 (2004) [Pisma Zh. Eksp. Teor. Fiz. **79**, 3 (2004)] [hep-ph/0311189].
- [29] A. D. Dolgov, S. L. Dubovsky, G. I. Rubtsov and I. I. Tkachev, Phys. Rev. D **88**, no. 11, 117701 (2013) [arXiv:1310.2376 [hep-ph]].
- [30] S. Davidson and M. E. Peskin, Phys. Rev. D **49**, 2114 (1994) [hep-ph/9310288].
- [31] H. Vogel and J. Redondo, JCAP **1402**, 029 (2014) [arXiv:1311.2600 [hep-ph]].
- [32] N. Vinyoles and H. Vogel, JCAP **1603**, 002 (2016) [arXiv:1511.01122 [hep-ph]].
- [33] J. D. Bowman, A. E. E. Rogers, R. A. Monsalve, T. J. Mozdzen and N. Mahesh, Nature **555** (2018) no.7694, 67.
- [34] J. B. Muoz and A. Loeb, Nature **557**, no. 7707, 684 (2018) [arXiv:1802.10094 [astro-ph.CO]].
- [35] R. Barkana, N. J. Outmezguine, D. Redigolo and T. Volansky, Phys. Rev. D **98**, no. 10, 103005 (2018) [arXiv:1803.03091 [hep-ph]].
- [36] A. Berlin, D. Hooper, G. Krnjaic and S. D. McDermott, Phys. Rev. Lett. **121**, no. 1, 011102 (2018) [arXiv:1803.02804 [hep-ph]].
- [37] E. D. Kovetz, V. Poulin, V. Gluscevic, K. K. Boddy, R. Barkana and M. Kamionkowski, Phys. Rev. D **98**, no. 10, 103529 (2018) [arXiv:1807.11482 [astro-ph.CO]].
- [38] K. K. Boddy, V. Gluscevic, V. Poulin, E. D. Kovetz, M. Kamionkowski and R. Barkana, Phys. Rev. D **98**, no. 12, 123506 (2018) [arXiv:1808.00001 [astro-ph.CO]].
- [39] N. Klop and S. Ando, Phys. Rev. D **98**, no. 10, 103004 (2018) [arXiv:1809.00671 [hep-ph]].
- [40] C. Creque-Sarbinowski, L. Ji, E. D. Kovetz and M. Kamionkowski, Phys. Rev. D **100**, no. 2, 023528 (2019) [arXiv:1903.09154 [astro-ph.CO]].
- [41] H. Liu, N. J. Outmezguine, D. Redigolo and T. Volansky, arXiv:1908.06986 [hep-ph].
- [42] E. Kou *et al.* [Belle II Collaboration], arXiv:1808.10567 [hep-ex].
- [43] Xiaolong Wang, <https://indico.ihep.ac.cn/event/9272/session/21/contribution/49/material/slides/0.pdf>
- [44] D. M. Asner *et al.*, Int. J. Mod. Phys. A **24**, S1 (2009) [arXiv:0809.1869 [hep-ex]].
- [45] Haiping Peng, <https://indico.inp.nsk.su/event/15/session/0/contribution/99/material/slides/0.pdf>
- [46] J. P. Lees *et al.* [BaBar Collaboration], Nucl. Instrum. Meth. A **726**, 203 (2013) [arXiv:1301.2703 [hep-ex]].
- [47] Z. Liu, Y. H. Xu and Y. Zhang, JHEP **1906**, 009 (2019) [arXiv:1903.12114 [hep-ph]].
- [48] Torben Ferber, https://indico.cern.ch/event/757995/contributions/3315335/attachments/1832761/3001940/2019_04_ferber_ALPS.pdf
- [49] P. f. Yin, J. Liu and S. h. Zhu, Phys. Lett. B **679**, 362 (2009) [arXiv:0904.4644 [hep-ph]].
- [50] <http://english.ihep.cas.cn/bes/doc/2250.html>
- [51] M. Ablikim *et al.* [BESIII Collaboration], Phys. Rev. D **96**, no. 11, 112008 (2017) [arXiv:1707.05178 [hep-ex]].
- [52] B. Aubert *et al.* [BaBar Collaboration], arXiv:0808.0017 [hep-ex].
- [53] R. Essig, J. Mardon, M. Papucci, T. Volansky and Y. M. Zhong, JHEP **1311**, 167 (2013) [arXiv:1309.5084 [hep-ph]].
- [54] Luca Pescatore, “Searching for New Physics in $b \rightarrow s l^+ l^-$ Transitions at the LHCb Experiment” (PhD thesis)

[55] The polar angle in the CM frame is related to that in the lab frame via $\tan \theta_{\text{cm}} = \sin \theta_{\text{lab}} / (\gamma \cos \theta_{\text{lab}} - \gamma\beta)$, where

$$\beta = 3/11 \text{ and } \gamma = 1/\sqrt{1 - \beta^2}.$$